MATHEMATICAL MODELING AND COMPUTING, Vol. 9, No. 2, pp. 187–202 (2022)

A new Lattice Boltzmann method for a Gray–Scott based model applied to image restoration and contrast enhancement

Alaa H.[1], Alaa N. E.[1], Aqel F.[2], Lefraich H.[3]

[1] *Laboratory LAMAI, Faculty of Science and Technology Cadi Ayyad University, 40000 Marrakesh, Morroco*

[2] *Computer, Networks, Mobility and Modeling laboratory (IR2M), Faculty of Sciences and Technics, Hassan First University of Settat, B.P. 577, Settat 26000, Morocco*

[3] *Laboratory MISI, Faculty of Sciences and Techniques, Hassan First University of Settat, B.P. 577, Settat 26000, Morocco*

(Received 4 May 2021; Revised 20 November 2021; Accepted 22 November 2021)

The aim of this work is to propose a new numerical approach to image restoration and contrast enhancement based on a reaction-diffusion model (Gray–Scott model). For noise removal, a Lattice Boltzmann technique is used. This method is usually used in fluid dynamics experiments. Since pixels motion can be compared to fluids motion, the presented technique also indicates a good performance in processing noisy images. The efficiency and performance of the proposed algorithm are verified by several numerical experiments.

Keywords: *image restoration, Lattice Boltzmann method, Gray–Scott model, reaction–diffusion, contrast enhancement, D2Q9 scheme, D2Q5 scheme.*

2010 MSC: 35K55, 35K57, 35G61, 68U10, 94A08 **DOI:** 10.23939/mmc2022.02.187

1. Introduction

The image processing is a discipline that allows analyzing, improvement, extraction or summarizing of information obtained from an image through the application of some algorithms. It has become an extensive field that has gone through significant development since its beginning. One can define the digital image processing as using the techniques that allow modification of a digital image, with the aim to improve or extract relevant information. The different techniques of image processing have become the most effective and rapidly used methods in wide range of areas, including artistic effects, medical visualization, industrial inspection, computer vision, etc. One of the most important fields in image processing is image restoration. This process aims at correction of degraded images and reconstruction of uncorrupted images from noisy or blurred ones.

The degradation of an image can be caused by different phenomena (measurement noise, camera shake, etc). The technique of image restoration consists in working on a degraded image to obtain a result similar to the original one.

Image restoration was one of the first techniques that attracted the attention of the research community. It seeks for correction of the distortions that occur during the emergence of a number of degradations. Among many different types of image degradations, two main types are encountered: spatial degradation or blurring, which is a form of reduction of bandwidth of an ideal image caused by imperfect image formation process, and point degradation or noise, which refers to the types of degradations where only the gray levels at the individual points are affected without introducing any blur.

In the recent decades, many research topics have been focussed on the study of partial equations and systems. The study of partial differential equations and systems had its origin in the eighteenth century by Laplace (gravitational potential fields) in 1780, and Fourier (analytic theory of heat) in

1822 as a central tool, and it is inspired by concrete models of mechanics. Later, the study of PDEs was also spurred by other physical or chemical problems (problems of diffusion theory, electrostatic, electricity or magnetism), biological (transport mechanisms in living cells) [1] and ecological problems, engineering problems and applied disciplines. Furthermore, the partial differential equations appeared as a natural tool to smooth images, and several applications in the field of image processing had been found, namely unconventional methods of processing [2].

PDE-based methods are considered as one of the most well founded mathematical techniques in image processing, especially in image restoration, contour detection and image denoising.

In the early 1990s, Perona and Malik proposed an unconventional noise filtering algorithm, based on differential equations modeling an anisotropic diffusion process [3]. Over the last 20 years, this algorithm has served as a reference since it has been widely used to perform medical image analysis, as well as astronomical image restoration. The major challenge in image restoration is to design methods, allowing the selective filtering of noise without affecting the interesting features of the original image. Perona and Malik proposed a diffusion penalty when the signal gradient is large.

They claimed to modify the diffusion equation to obtain the anisotropic diffusion, replacing the linear diffusion by a nonlinear one. The proposed approach consists in smoothing the homogeneous regions while preserving the edges. The general form of the used equation is the following

$$\frac{\partial u}{\partial t} = \operatorname{div}(g(|\nabla u|)\nabla u),$$

where they proposed two different forms of function g with a diffusion threshold k, given by

$$g_1(|\nabla u|) = \exp\left(-\frac{|\nabla u|^2}{k^2}\right) \quad \text{and} \quad g_2(|\nabla u|) = \frac{1}{1+\frac{|\nabla u|^2}{k^2}}.$$

The scale-spaces generated by these functions are different, the first privileges high-contrast edges over low-contrast ones, while the second privileges wide regions over smaller ones [3].

Later on, Alvarez et al. [4] had proposed a stable algorithm for image restoration based on "the mean curvature motion" equation. The proposed model is given by the following nonlinear parabolic equation

$$\frac{\partial u}{\partial t} = g(|G * Du|)|Du| \operatorname{div}\left(\frac{Du}{|Du|}\right), \quad u(0,x,y) = u_0(x,y). \tag{1}$$

We denote by $u_0(x,y)$, the grey level of the image to be processed, $u(t,x,y)$ is its smoothed version, G is a smoothing kernel (for instance, a gaussian kernel) and $g(s)$ is a nonincreasing function that tends to zero when s tends to infinity. Alvarez et al. proved existence and uniqueness of the viscosity solution of the associated parabolic equations, and they showed the numerical scheme and some experimental results.

The new version of Perona and Malik model theory for the edge detection and image restoration, was proposed by Catté et al. in 1992 [5]. They proposed a regularization of image gradient in order to obtain a well-posed model, the considered model was given by the following nonlinear equation

$$\begin{cases} \dfrac{\partial u}{\partial t} - \operatorname{div}(g(|\nabla G_\sigma * u|)\nabla u) = 0 & \text{in } (0,T)\times\Omega, \\ \dfrac{\partial u}{\partial n} = 0 & \text{in } (0,T)\times\partial\Omega, \\ u(0,x) = u_0(x) & \text{in } \Omega. \end{cases} \tag{2}$$

Where the initial data u_0 belongs to $L^2(\Omega)$, g is a nonnegative decreasing function defined by

$$g(t) = \frac{1}{1+t^2}, \tag{3}$$

such that

$$g(0) = 1, \quad \lim_{t\to+\infty} g(t) = 0 \quad \text{and} \quad t \to g(\sqrt{t}) \quad \text{is smooth}$$

and $|\nabla G_\sigma * u|$ is given by

$$|\nabla G_\sigma * u| = \sqrt{\sum_{i=1}^{2} \left(\frac{\partial G_\sigma}{\partial x_i} * \overline{u} \right)^2},$$

where $G_\sigma(x) = C\sigma^{-\frac{1}{2}} \exp\left(\frac{-x^2}{4\sigma}\right)$ and $\overline{u}$ is a linear and continuous extension of u to $\mathbb{R}^2$. Catté et al. [5] proved existence, uniqueness and regularity of solutions is $C([0,T], L^2(\Omega)) \cap L^2(0,T; H^1(\Omega))$. Also, they described briefly the proposed numerical method, where they found that experimental results on pictures were not different from those obtained by the Perona and Malik.

In 2009, Morfu [6] showed that nonlinear diffusion processes are ruled by the Fisher equation. This equation describes the transport mechanism in living cells, and it allows performing contrast enhancement [7], noise filtering, though involves a blurry image [8, 9].

In 2014 [10], a new processing algorithm based on anisotropic diffusion and nonlinear process was suggested to remove the noise and enhance the image. The main idea of this method was to modify the model of S. Morfu [8]. During the calculation of the anisotropic diffusion coefficient, a Gaussian filter on the image gradient was applied, and the threshold parameter of gradient according to the gradient of the image at each iteration, was chosen. The proposed model is given by:

$$\begin{cases} \dfrac{\partial u(t,x)}{\partial t} = \operatorname{div}(g(|G_\sigma * \nabla u|, \lambda)\nabla u(t,x)) + f(u), & (t,x) \in (0,T) \times \Omega, \\ \dfrac{\partial u}{\partial n} = 0, & (t,x) \in (0,T) \times \partial\Omega, \\ u(0,x) = u_0(x), & x \in \Omega, \end{cases} \tag{4}$$

where the nonlinearity $f(u)$ is commonly chosen cubic (Nagumo et al., 1962; Fitzhugh, 1961). It is defined by the following sense

$$f(u) = \beta u(u-\alpha)(1-u).$$

One of the significant broadly utilized numerical approaches to solve finite PDE's in image processing, is the finite difference method (FDM) using an explicit scheme (this is due to the structure of digital images, which are formed by a set of uniformly distributed pixels). This explicit scheme needs a small-time step to be stable, and thus a large number of iterations is necessary. The treatment of complex boundary conditions also presents significant difficulties in the use of FDM. Some adaptive and semi-implicit operator splitting schemes were used, but parallelization of these methods is difficult. Consequently, such traditional numerical methods lack efficiency and may also provoke an obvious boundary effect.

For this purpose, we propose a new approach to image restoration and contrast enhancement, based on the Lattice Boltzmann method (LBM).

Lattice Boltzmann method is a numerical method relatively new, compared to classical approaches used in numerical simulation. It is derived from the kinetic theory of gases, established by Boltzmann and which was first proposed in 1973 by Hardy et al. [11].

The Lattice Boltzmann method is widely used in the fields of fluid dynamics [12–15]. The LBM can be regarded as the discrete format of the continuous Boltzmann equation. In other words, LBM is a mesoscopic approach that simulates a macroscopic phenomenon governed by partial differential equation problems [16, 17]). It is characterized by its simple calculation procedure, simple and efficient implementation of the computer code, high accuracy (It allows to model physical phenomena on a small scale with high accuracy). Implicit computation of curvatures, simple implementation of boundary conditions as well as its direct discretization and computational capacity [18].

Generally, the LBM compared to the other classical numerical methods, only includes two simple phases: the first one is collision and the second one is streaming, where particles move on the lattice according to the directional velocities.

In the framework of image analysis, myriads of works in image processing were achieved by adapting the Lattice Boltzmann method. It is implemented to perform image segmentation, image dithering,

image boundary detection and denoising operation. In 1999, Jawerth et al. [19] were the first to adopt the LBM to solve the Perona and Malik equation. It was noticed that the LBM was feasible and efficient in the study of image processing. After that, a new LBM-based active contour and level set (LS) methods had been developed and implemented for the study of image segmentation and edge detection [20, 21]. Thereafter, Chang and Yang [22] presented a Lattice Boltzmann model for image denoising. They found that the computational speed of LBM was much faster than that of the iterative fixed point method.

Finally in [23], a new Lattice Boltzmann model for the Ambrosio and Tortorelli model [24], was proposed for the study of image filtering and contour detection.

The main objective of this paper is to compare the difference in filtering effect between two models $D2Q5$ (two dimensions and five discrete velocity directions), and $D2Q9$ (two dimensions and nine discrete velocity directions) of the proposed system. The filtering effect difference is evaluated through testing a set of images, featuring different degrees of contrast, edge detail, texture, etc.

By taking into account the effect of the noise type on the results, three types of noise are added to each image which are pepper and salt noise, Gaussian noise and speckle noise, respectively. The high level of performance of the $D2Q9$ model is proved by comparing and utilizing many criteria, including the calculated error on the restored image at each time step iteration, the line profile, and the EME/PSNR values of each result.

In this paper, a new Lattice Boltzmann method for the Gray–Scott based model applied in image restoration and contrast enhancement, is introduced in section 2. Numerical experiments are shown in section 3. In section 4, the obtained results and the discussions are presented and finally, a brief conclusion is given in section 5.

2. Lattice–Boltzmann method for reaction-diffusion system

Note that since 1990, the Perona–Malik algorithm has been extensively used for medical image analysis and restoration of astronomical images. Numerous systems have been proposed including the following reaction-diffusion system:

$$\begin{cases} \dfrac{\partial u}{\partial t} = D_u \Delta u + F(u,v), \\ \dfrac{\partial v}{\partial t} = D_v \Delta v + G(u,v), \end{cases} \tag{5}$$

where Δ represents the Laplacian, u and v are the concentrations of activator and inhibitor, while D_u and D_v are the diffusion coefficients. The functions F and G describe the rate of production of the activator and initiator.

In the case where $F(u,v) = \beta u(u-a)(1-u) - v$ and $G(u,v) = u - bv$, the system corresponds to the model of Fitzhugh–Nagumo reaction diffusion equations, which is utilized to detect edges for binary images [25]. Further types of reaction functions F and G can be considered, i.e. the Brusselator model to perform texture synthesis [26, 27], as well as the Oregonator model of the Belousov–Zhabotinsky reaction to perform mathematical morphology operations [2].

In this work, we are interested in the derivation of the following nonlinear reaction-diffusion system from the Lattice Boltzmann equation:

$$\begin{cases} \dfrac{\partial u}{\partial t} - \operatorname{div}(\alpha(|\nabla u|, \lambda(t))\nabla u) = F(u,v) & \text{in } (0,T)\times\Omega, \\ \dfrac{\partial v}{\partial t} - d_v \Delta v = G(u,v) & \text{in } (0,T)\times\Omega, \\ \dfrac{\partial u}{\partial n} = \dfrac{\partial v}{\partial n} = 0 & \text{in } (0,T)\times\partial\Omega, \\ u(0) = u_0, \quad v(0) = v_0 & \text{in } \Omega. \end{cases} \tag{6}$$

The diffusivity α is a decreasing and nonnegative function that satisfies

$$\alpha(0,\lambda(t)) = 1 \quad \text{and} \quad \lim_{s\to+\infty} \alpha(s,\lambda(t)) = 0, \tag{7}$$

where $|\nabla u| = \sqrt{\sum_{i=1}^{2} \left(\frac{\partial u}{\partial x_i}\right)^2}$ is the euclidian norm of gradient of u. The conditions on α are interpreted as follows: in low gradient areas, the Perona–Malik model behaves like a heat equation, while in high gradient areas, diffusion is stopped and edge preservation is guaranteed. In 1998, Black et al. [28] suggested the following function:

$$\alpha(s,\lambda(t)) = \frac{1}{1+\frac{s^2}{\lambda^2(t)}}.$$

The parameter $\lambda(t)$ was chosen as a function depending on time:

$$\lambda(t) = \frac{1.4826}{\sqrt{2}}\,\mathrm{MAD}(|\nabla u(t)|),$$

MAD denotes the median absolute deviation which can be calculated as:

$$\mathrm{MAD}(|\nabla u(t)|) = \mathrm{median}\left(|\nabla u(t) - \mathrm{median}(|\nabla u(t)|)|\right)$$

where median$(|\nabla u(t)|)$ represents the median value over the image u of gradient norm. According to Gray–Scott model, the nonlinearity functions F and G are defined as follows:

$$\begin{cases} F(u,v) = -u\,v^2 + A(1-u), \\ G(u,v) = u\,v^2 - B\,v, \end{cases}$$

where A and B are constants.

The Lattice Boltzmann method (LBM), as a numerical approach developed from the fluid kinetic theory or the lattice gas, is one of the methods used in image processing. It is considered good enough to solve complex boundaries and it can reduce all statistical noise in the resulting image.

In lattice gases, particles reside on nodes of a discrete lattice and move to their nearest neighbors along links, while in image processing, the particles can be viewed as pixels. In Lattice Boltzmann simulation, pixels move from one lattice node to another. During propagation, pixels may collide with their neighbors (pixels) to reach a different value.

The evolution equations' of density distribution function in Lattice boltzmann method with BGK (Bhatnagar–Gross–Krook) approximation [12], can be expressed as:
for all $0 \leqslant i \leqslant l$

$$f_i(x + c_i dt_1, t + dt_1) - f_i(x,t) = \frac{-1}{\tau_f}\left(f_i(x,t) - f_i^{(eq)}(x,t)\right) + dt_1 \bar{w}_i F, \tag{8}$$

$$g_i(x + c_i dt_2, t + dt_2) - g_i(x,t) = \frac{-1}{\tau_g}\left(g_i(x,t) - g_i^{(eq)}(x,t)\right) + dt_2 \bar{z}_i G. \tag{9}$$

Where f_i and g_i are the density distribution functions of particles along the i^{th} direction. $f_i(x,t)$ and $g_i(x,t)$ are the distribution functions of particles with discrete velocity c_i at position x and time t. dt_1 and dt_2 are the streaming time step, τ_f and τ_g are the single relaxation parameters in the BGK model, and the quantities $f_i(x,t)$ and $g_i(x,t)$ are the density distribution functions of particles at position x and time t along the i^{th} direction.

The weight coefficients $\bar{w}_i$ and $\bar{z}_i$ satisfy the following constraints,

$$\sum_{i=0}^{l} \bar{w}_i = \sum_{i=0}^{l} \bar{z}_i = 1.$$

Where l is set to be 8 for $D2Q9$ model and 4 for $D2Q5$.

The equilibrium density distribution functions $f_i^{(\mathrm{eq})}$ and $g_i^{(\mathrm{eq})}$ along the i^{th} direction, are expressed as:

$$\begin{aligned} f_i^{(\mathrm{eq})}(x,t) &= \alpha_i u(x,t), \\ g_i^{(\mathrm{eq})}(x,t) &= \alpha_i v(x,t). \end{aligned} \tag{10}$$

For $D2Q5$ Model, the discrete velocity directions are given by:

$$c_i = \begin{cases} (0,0), & i = 0, \\ \left(\cos\dfrac{(i-1)\pi}{2}, \sin\dfrac{(i-1)\pi}{2}\right) c, & i = 1,2,3,4, \end{cases}$$

where $c = \frac{\Delta x}{\Delta t}$ and Δx is the lattice spacing.

The weight α_i is defined by:

$$\alpha_i = \frac{1}{5} \quad \text{for} \quad i = 0,1,2,3,4.$$

The discrete velocity directions for the $D2Q9$ model are defined as follows:

$$c_i = \begin{cases} (0,0), & i = 0, \\ \left(\cos\dfrac{(i-1)\pi}{2}, \sin\dfrac{(i-1)\pi}{2}\right) c, & i = 1,2,3,4, \\ \left(\cos\left(\dfrac{(i-5)\pi}{2} + \dfrac{\pi}{4}\right), \sin\left(\dfrac{(i-5)\pi}{2} + \dfrac{\pi}{4}\right)\right) \sqrt{2}\, c, & i = 5,6,7,8, \end{cases}$$

and the weight α_i is given by

$$\alpha_i = \begin{cases} \dfrac{4}{9}, & i = 0, \\ \dfrac{1}{9}, & i = 1,2,3,4, \\ \dfrac{1}{36}, & i = 5,6,7,8. \end{cases}$$

Note that $\sum_{i=0}^{l} \alpha_i = 1$, and

$$\begin{cases} \displaystyle\sum_{i=0}^{l} f_i = \sum_{i=0}^{l} f_i^{(\mathrm{eq})}, \\ \displaystyle\sum_{i=0}^{l} g_i = \sum_{i=0}^{l} g_i^{(\mathrm{eq})} \end{cases} \tag{11}$$

The macroscopic quantities u and v satisfy the following properties

$$\begin{cases} u(x,t) = \displaystyle\sum_{i=0}^{l} f_i = \sum_{i=0}^{l} f_i^{(\mathrm{eq})}, \\ v(x,t) = \displaystyle\sum_{i=0}^{l} g_i = \sum_{i=0}^{l} g_i^{(\mathrm{eq})}, \end{cases} \tag{12}$$

and

$$\begin{cases} \displaystyle\sum_{i=0}^{l} c_i f_i^{(\mathrm{eq})} = 0, \quad \sum_{i=0}^{l} c_i c_i f_i^{(\mathrm{eq})} = c_s^2 u I, \\ \displaystyle\sum_{i=0}^{l} c_i g_i^{(\mathrm{eq})} = 0, \quad \sum_{i=0}^{l} c_i c_i g_i^{(\mathrm{eq})} = c_s^2 v I, \end{cases} \tag{13}$$

where c_s designates the speed of sound which depends on the chosen lattice. For $D2Q9$ and $D2Q5$ model, the square of c_s satisfies $c_s^2 = \frac{c^2}{3}$ and $c_s^2 = \frac{2c^2}{5}$, respectively.

In order to recover the equations of system (6), two essential steps are used. First, we use the Taylor expansion in time and space to (8), we obtain the following system

$$\begin{cases} D_i f_i + \dfrac{dt_1}{2} D_i^2 f_i = \dfrac{1}{\tau_f dt_1}\left(f_i^{(\mathrm{eq})} - f_i\right) + \bar{w}_i F, \\ D_i g_i + \dfrac{dt_2}{2} D_i^2 g_i = \dfrac{1}{\tau_g dt_2}\left(g_i^{(\mathrm{eq})} - g_i\right) + \bar{z}_i G, \end{cases} \tag{14}$$

where $D_i = \partial_t + c_i \cdot \nabla$.

The second step is based on the so-called Chapman–Enskog procedure

$$\begin{cases} f_i = f_i^{(\mathrm{eq})} + \varepsilon f_i^{(1)} + \varepsilon^2 f_i^{(2)}, \\ g_i = g_i^{\mathrm{eq}} + \varepsilon g_i^{(1)} + \varepsilon^2 g_i^{(2)}, \\ \partial_t = \varepsilon \partial_{t_1} + \varepsilon^2 \partial_{t_2}, \\ \nabla = \varepsilon \nabla_1, \quad F = \varepsilon^2 F^{(2)}, \quad G = \varepsilon^2 G^{(2)}. \end{cases} \tag{15}$$

Where ε is a small expansion parameter, $t_1 = \frac{t}{\varepsilon}$ and $t_2 = \frac{t}{\varepsilon^2}$ are two macroscopic time scales and ∇_1 is the gradient operator in the macroscopic length scale $x_1 = \frac{x}{\varepsilon}$.

Note that the system equations (6) are recovered following the same steps. First, we reconstruct the first equation. To do this, we sum the first formula in (15) over i and we use the first equality in (10) to get

$$\sum_{i=0}^{l} f_i^{(k)} = 0 \quad (k \geqslant 1). \tag{16}$$

By substituting (15) into (14), and then treating the terms in order of ε and ε^2 separately, one obtain

$$D_{1i} f_i^{(\mathrm{eq})} = -\frac{1}{\tau_f dt_1} f_i^{(1)}, \tag{17}$$

$$\partial_{t_2} f_i^{(\mathrm{eq})} + D_{1i} f_i^{(1)} + \frac{dt_1}{2} D_{1i}^2 f_i^{(\mathrm{eq})} = \frac{-1}{\tau_f dt_1} f_i^{(2)} + \bar{w}_i F^{(2)}, \tag{18}$$

where $D_{1i} = \partial_{t_1} + c_i \cdot \nabla_1$.

By applying (17) to the left side of (18) and combining the terms including $f_i^{(1)}$ on the left side, one can rewrite the equation (18) as follows

$$\partial_{t_2} f_i^{(\mathrm{eq})} + \left(1 - \frac{1}{2\tau_f}\right) D_{1i} f_i^{(1)} = \frac{-1}{\tau_f dt_1} f_i^{(2)} + \bar{w}_i F^{(2)}. \tag{19}$$

Now, we sum the equation (19) over i and we use (16), we obtain

$$\partial_{t_2} u + \left(1 - \frac{1}{2\tau_f}\right) \sum_{i=0}^{l} (\partial_{t_1} + c_i \nabla_1) f_i^{(1)} = F^{(2)}. \tag{20}$$

The term $\partial_{t_1} u$ is equal to 0. Indeed, if we sum the equation (17) over i, we get

$$\sum_{i=0}^{l} D_{1i} f_i^{(\mathrm{eq})} = 0.$$

Using the definition of D_{1i}, it follows that

$$\partial_{t_1} u + \sum_{i=0}^{l} c_i \nabla f_i^{(\mathrm{eq})} = 0,$$

and then we obtain the desired result. Next, by multiplying (17) by c_i and summing over i, one can

write

$$\sum_{i=0}^{l} c_i f_i^{(1)} = -\tau_f dt_1 \sum_{i=0}^{l} c_i D_{1i} f_i^{(\mathrm{eq})}.$$

Since

$$\sum_{i=0}^{l} c_i D_{1i} f_i^{(\mathrm{eq})} = \partial_{t_1} \left(\sum_{i=0}^{l} c_i f_i^{(\mathrm{eq})} \right) + \nabla_1 \left(\sum_{i=0}^{l} c_i c_i f_i^{(\mathrm{eq})} \right)$$

Using formula (13) and the fact that $\partial_{t_1} u = 0$, we obtain

$$\sum_{i=0}^{l} c_i D_{1i} f_i^{(\mathrm{eq})} = c_s^2 \nabla_1 u.$$

Consequently,

$$\sum_{i=0}^{l} c_i f_i^{(1)} = -\tau_f dt_1 c_s^2 \nabla_1 u. \tag{21}$$

Then substituting (21) into (20), we have

$$\partial_{t_2} u - \nabla_1 \left(dt_1 \, c_s^2 \left(\tau_f - \frac{1}{2} \right) \nabla_1 u \right) = F^{(2)}. \tag{22}$$

Therefore, multiplying (22) by ε^2, it follows that

$$\partial_t u - \nabla \left(dt_1 \, c_s^2 \left(\tau_f - \frac{1}{2} \right) \nabla u \right) = F. \tag{23}$$

Similarly, we obtain

$$\partial_t v - \nabla \left(dt_2 \, c_s^2 \left(\tau_g - \frac{1}{2} \right) \nabla v \right) = G, \tag{24}$$

where the coefficient d is expressed in term of the relaxation time τ by the following sense

$$d = \left(\tau - \frac{\Delta t}{2} \right) c_s^2.$$

The function α and the diffusion coefficient d_v and the single relaxation parameters τ_f and τ_g, are related as follows

$$\alpha = dt_1 \, c_s^2 \left(\tau_f - \frac{1}{2} \right) \tag{25}$$

and

$$d_v = dt_2 \, c_s^2 \left(\tau_g - \frac{1}{2} \right). \tag{26}$$

The coupled reaction-diffusion equations (6) are recovered by combining (23)–(24):

$$\begin{cases} \dfrac{\partial u}{\partial t} - \operatorname{div}(\alpha \nabla u) = F(u, v), \\ \dfrac{\partial v}{\partial t} - d_v \Delta v = G(u, v), \\ u(0) = u_0, \quad v(0) = v_0, \\ \dfrac{\partial u}{\partial n} = \dfrac{\partial v}{\partial n} = 0. \end{cases} \tag{27}$$

3. Numerical experiments

In this section, we derive an efficient numerical approach to image restoration and contrast enhancement. The main idea is to solve (27) using the Lattice Boltzmann model, where the overall procedure of the proposed method is shown in Algorithm 1. Prior to the computation, it is necessary to calculate the parameter λ, and the relaxation time τ_f which is related to $\alpha(|\nabla u|)$.

To calculate ∇u in the internal region of the image for $D2Q5$ and $D2Q9$ models, the following formula is used:

$$\nabla u(x) = \frac{1}{\beta \Delta x} \sum_{i=0}^{l} e_i u(x + c_i dt), \tag{28}$$

where $\Delta x = 1$ and β is fixed at 6.0 and 2.0 for $D2Q9$ and $D2Q5$ models, respectively. l is set to be 8 for $D2Q9$ model and 4 for $D2Q5$ and the vector $e_i = \frac{c_i}{c}$.

Hence, the variable τ_f is computed from equation (25) as:

$$\tau_f = \frac{\gamma\, dt_1}{1 + \frac{|\nabla u|^2}{\lambda^2(t)}} + \frac{1}{2}, \tag{29}$$

where γ is a constant which is set to be 2.5 and 3.0, respectively, for $D2Q5$ and $D2Q9$ models.

It is well known that the stability of the Lattice Boltzmann method, requires the following condition: $\tau_f > \frac{1}{2}$.

Furthermore, the parameter $\lambda(t)$ is calculated at each iteration by

$$\lambda(t) = \frac{1.4826}{\sqrt{2}}\, \mathrm{MAD}(|\nabla u(t)|). \tag{30}$$

This parameter will be used in order to determine the stopping time of our algorithm, and also to estimate the noise level in the image.

Algorithm 1 The LBM algorithm for the proposed reaction-diffusion system.

Initialization: u_0, v_0, $f_i^{(0)}$, $g_i^{(0)}$, λ^0, d_v, $f_i^{(\mathrm{eq})}$, $g_i^{(\mathrm{eq})}$, $\bar{w}$, $\bar{z}$, dt_1, dt_2, F, G.
While $\left\|\lambda^{(k+1)} - \lambda^{(k)}\right\| > \varepsilon$ **do**
1. **For** $k = 1, 2, 3, \ldots,$ **do**
2. **Compute** $\nabla u^{(k)}$ **by the equation** (21).
3. **Calculate** $\lambda^{(k)}$, α, τ **via Eq**. (25), (29) and (30).
4. **Collision:**

$$f_i^{(k)}(x,t) = f_i^{(k)}(x,t) - \frac{1}{\tau_f}\left(f_i^{(k)}(x,t) - f_i^{(\mathrm{eq})^{(\mathrm{k})}}(x,t)\right) + dt_1 \bar{w}_i F^{(k)},$$
$$g_i^{(k)}(x,t) = g_i^{(k)}(x,t) - \frac{1}{\tau_g}\left(g_i^{(k)}(x,t) - g_i^{(\mathrm{eq})^{(\mathrm{k})}}(x,t)\right) + dt_2 \bar{z}_i G^{(k)}.$$

5. **Streaming:**

$$f_i^{(k+1)}(x + c_i dt_1, t + dt_1) = f_i^{(k)}(x,t),$$
$$g_i^{(k+1)}(x + c_i dt_2, t + dt_2) = g_i^{(k)}(x,t).$$

6. **Compute:** $u^{(k)} = \sum_i f_i^{(k)}$ **and** $v^k = \sum_i g_i^{(k)}$.
7. **End for**: when the convergent rule is met.
End while.

4. Results and discussions

In this section, some original images are selected (see Figure 1), and different types of noise are added to them using Mathlab: a Gaussian noise with an average value of 0 and a variance of 0.01, salt and pepper noise with an intensity of 0.05, or speckle noise with an average value of 0 and a variance of 0.04.

The comparison of image restoration of both $D2Q5$ and $D2Q9$ models, is ensured using several criteria, namely the error evaluated on the restored image at each time step iteration, the line profile, and the EME image enhancement which measures the image contrast by calculating the quantity

$$\mathrm{EME} = \frac{1}{k_1 k_2} \sum_{l=1}^{k_1} \sum_{k=1}^{k_2} 20 \log_{10} \frac{u^w_{\max,k,l}}{u^w_{\min,k,l}},$$

where the image $u(N, M)$ is divided into $k_1 k_2$ blocks $w_{k,l}(i, j)$ of sizes $l_1 l_2$. $u^w_{\max,k,l}$ and $u^w_{\min,k,l}$ are respectively maximum and minimum values of the image $u(N, M)$ inside the block $w_{k,l}$. A higher value of EME indicates that the image is enhanced very well.

In addition, an objective criterion is used to give an idea about the quality of the filtered image. In general, the PSNR is used in the image restoration to validate the filtering model. This criterion is adapted as follows

$$\mathrm{MSE} = \frac{1}{MN} \sum_{i=1}^{M} \sum_{j=1}^{N} \left[U(i, j) - U_0(i, j)\right]^2,$$

$$\mathrm{PSNR} = 10 \log_{10} \frac{255^2}{\mathrm{MSE}},$$

where U is the restored image with enhancement and U_0 is the original image.

In the following numerical experiments, different images to which different types of noise were added, are processed using the $D2Q9$ and $D2Q5$ models.

Fig. 1. Different original images.

The restoration results using $D2Q5$ and $D2Q9$ models are illustrated in Figures 2–4, 6, 10–13 as well as the comparison in Figures 5, 9 and Table 1.

It is well known that salt-and-pepper noise is generally more difficult to remove than Gaussian and speckle noise. Note that the processed versions of the images corrupted by this type of noise, which were obtained by the proposed models, contain no noise points and are well enhanced.

From the result above, the restored image obtained by the $D2Q9$ model is more enhanced, and better recovered than the one processed by the $D2Q5$ model, since it removes noise without removing image structures such as textures and edges.

In order to see the difference between the two models more accurately, we show the evolution of the error calculated for the restored images, at each time step iteration, obtained by these two latter.

We remark that the error corresponding to the restored image using $D2Q9$ model, decreases more quickly with time iteration than the other calculated by $D2Q5$ model. Thus, a part of the noise is still preserved on the image processed by the $D2Q5$ model.

If we look at the restored image corresponding to the $D2Q5$ model, the presence of noise and blur effects is noticeable. These effects are not seen in the restored image of the $D2Q9$ model. In order

Fig. 2. Left: Noisy image by a gaussian noise, restored image obtained by the proposed model: **Middle:** $D2Q5$ model. **Right:** $D2Q9$ model.

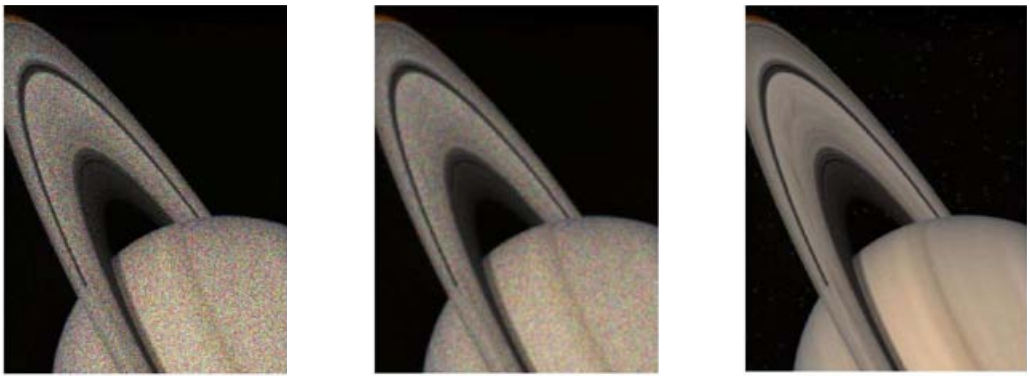

Fig. 3. Left: Noisy image by speckle noise, restored image obtained by the proposed model: **Middle:** $D2Q5$ model. **Right:** $D2Q9$ model.

Fig. 4. Left: Noisy image by salt and pepper noise, restored image obtained by the proposed model: **Middle:** $D2Q5$ model. **Right:** $D2Q9$ model.

to see the performance of the $D2Q9$ model, we represent a line profile for the original and restored images. More specifically, the red curve corresponds to the original image, while the restored image obtained using the $D2Q9$ model, is represented by the blue curve.

The line profile of the restored image follows simultaneously the original profile, which means that the $D2Q9$ model restores, and enhances the image contrast very well without eliminating the image information.

In order to evaluate the image quality, in the following table we present EME and PSNR values of each restored image using $D2Q5$ and $D2Q9$ models.

The value of these statistical measures increases when the restored image approaches to the original one. This result explains why the $D2Q9$ model consistently has a high value of EME and PSNR compared to the values obtained by the $D2Q5$ model. Based on this result, we can say that the images processed by $D2Q9$ model are as clear as those restored by $D2Q5$ model.

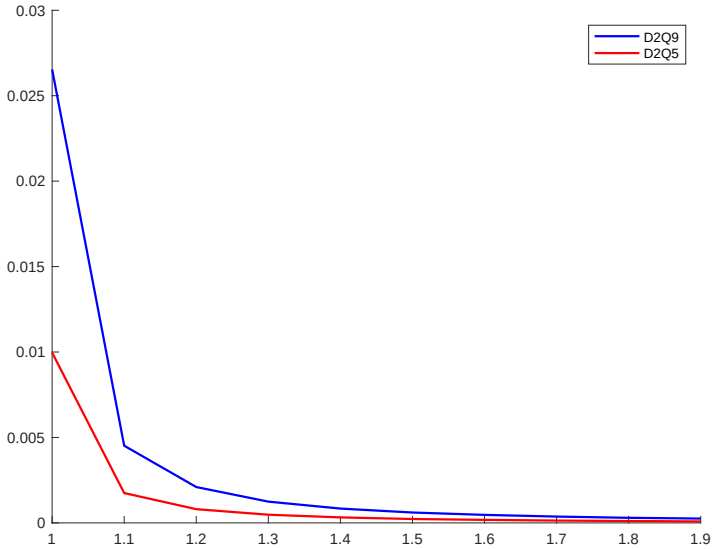

Fig. 5. Error graph calculated for restored Saturn image by the proposed model; X axis: time step dt, Y axis: $\|\lambda^{n+1} - \lambda^n\|$.

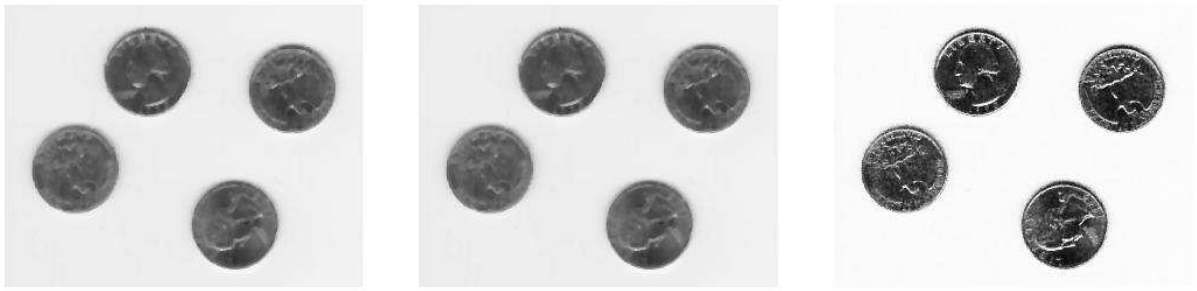

Fig. 6. Left: Noisy image using Gaussian noise, restored image obtained by the proposed model: **Middle:** $D2Q5$ model. **Right:** $D2Q9$ model.

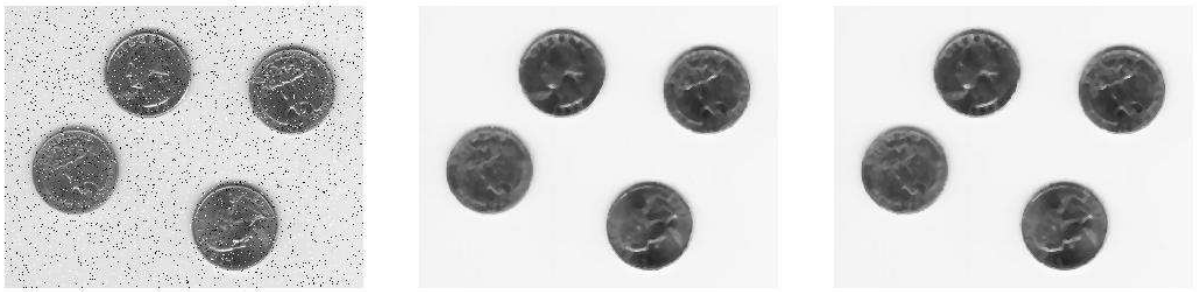

Fig. 7. Left: Noisy image by salt and pepper noise, restored image obtained by the proposed model. **Middle:** $D2Q5$ model. **Right:** $D2Q9$ model.

Fig. 8. Left: Noisy image by speckle noise, Restored image obtained by the proposed model: **Middle:** $D2Q5$ model. **Right:** $D2Q9$ model.

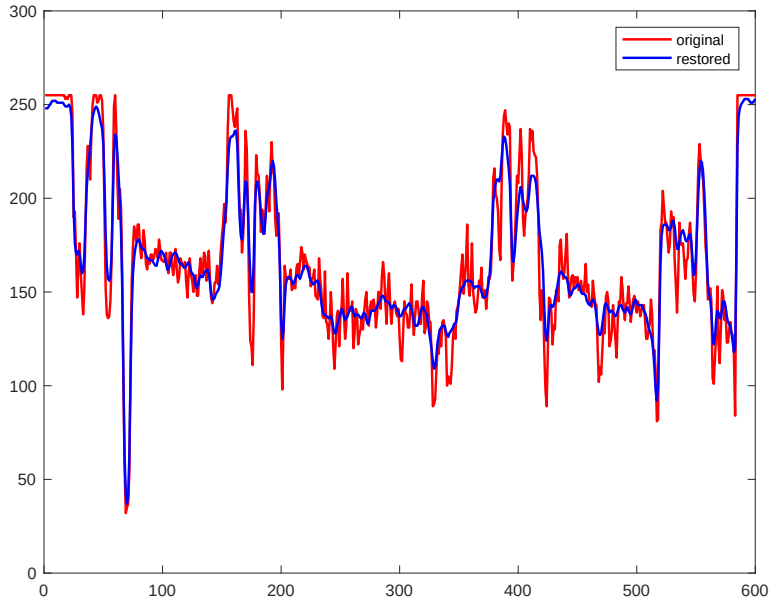

Fig. 9. Line profile number 250. **Red:** Original image. **Blue:** restored image by using the $D2Q9$ model. X and Y axis represents respectively X and Y coordinates of pixel value of Line 250.

Fig. 10. Left: Noisy image by a Gaussian noise, restored image obtained by the proposed model. **Middle:** $D2Q5$ model. **Right:** $D2Q9$ model.

Fig. 11. Left: Noisy image by salt and pepper noise, restored image obtained by the proposed model. **Middle:** $D2Q5$ model. **Right:** $D2Q9$ model.

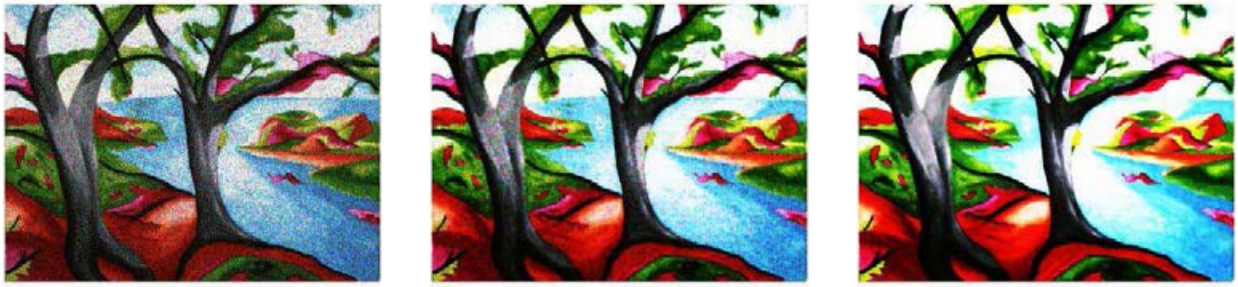

Fig. 12. Left: Noisy image by speckle noise, restored image obtained by the proposed model. **Middle:** $D2Q5$ model. **Right:** $D2Q9$ model.

Fig. 13. Left: Noisy image by salt and pepper noise, restored image obtained by the proposed model. **Middle:** $D2Q5$ model. **Right:** $D2Q9$ model.

Table 1. EME and PSNR values of both restored image by $D2Q5$ and $D2Q9$ models.

Images	**EME and PSNR values**	**Type of models**	
		$D2Q5$ **Model**	$D2Q9$ **Model**
Example 1	EME	5.82	7.39
	PSNR	75.27	76.82
Example 2	EME	10.82	12.20
	PSNR	71.70	72.12
Example 3	EME	11.09	12.64
	PSNR	72.62	73.67

5. Conclusion

In the present work, the Lattice Boltzmann method is applied to solve a new reaction-diffusion system. This system is adapted to image filtering and contrast enhancement. The $D2Q5$ and $D2Q9$ models are used to restore several images with three different types of noise. From the above evaluation, it has been proved that $D2Q9$ model gives satisfactory results in image restoration and enhancement compared to $D2Q5$ model, which is less effective in processing of the corrupted images. Note that the high performance of the $D2Q9$ model will be very useful to process a large amount of image data. Furthermore, the Lattice Boltzmann method is efficient for recovering an image to which different types of noise have been added.

[1] Murray J.-D. Mathematical biology. Berlin, Springer (1989).

[2] Teuscher C., Adamatzky A. Proc. of the 2005 Workshop on Unconventional Computing From cellular Automata to Wetwar. Luniver Press Beckington (2005).

[3] Perona P., Malik J. Scale-space and edge detection using anisotropic diffusion. IEEE Transactions on Pattern Analysis and Machine Intelligence. **12** (7), 629–639 (1990).

[4] Alvarez L., Lions P.-L., Morel J. M. Image Selective Smoothing and Edge Detection by Nonlinear Diffusion. II. SIAM Journal on Numerical Analysis. **29** (3), 845–866 (1992).

[5] Catté F., Lions P-L., Morel J.-M., Coll T. Image selective smoothing and edge detection by nonlinear diffusion. SIAM Journal on Numerical Analysis. **29** (1), 182–193 (1992).

[6] Morfu S. On some applications of diffusion processes for image processing. Physics Letters A. **373** (29), 2438–2444 (2009).

[7] Alaa K., Atounti M., Zirhem M. Image restoration and contrast enhancement based on a nonlinear reaction-diffusion mathematical model and divide & conquer technique. Mathematical Modeling and Computing. **8** (3), 549–559 (2021).

[8] Morfu S., Marquié P., Nofiélé B., Ginhac D. Chapter 3 – Nonlinear systems for image processing. Advances in Imaging and Electron Physics. **152**, 79–151 (2008).

[9] Morfu S., Nofiele B., Marquié P. On the use of multistability for image processing. Physics Letters A. **367** (3), 192–198 (2007).

[10] Oussous M. A., Alaa N., Khouya Y. A. Anisotropic and nonlinear diffusion applied to image enhancement and edge detection. International Journal of Computer Applications in Technology. **49** (2), 122–133 (2014).

[11] Hardy J., Pomeau Y., de Pazzis O. Time evolution of a two-dimensional model system. I. Invariant states and time correlation functions. Journal of Mathematical Physics. **14** (12), 1746–1759 (1973).

[12] Chen S., Doolen G. D. Lattice Boltzmann method for fluid flows. Annual Review of Fluid Mechanics. **30** (1), 329–364 (1998).

[13] Wolf–Gladrow D. A. Lattice Gas Cellular Automata and Lattice Boltzmann Models. Springer–Verlag, Berlin–Heidelberg (2000).

[14] Shan X. Simulation of Rayleigh–Bénard convection using a lattice Boltzmann method. Physival Review E. **55** (3), 2780–2788 (1997).

[15] Ho J.-R., Kuo C.-P., Jiaung W.-S., Twu C.-J. Lattice Boltzmann scheme for hyperbolic heat conduction equation. Numerical Heat Transfer, Part B: Fundamentals. **41** (6), 591–607 (2002).

[16] Shi B., Deng B., Du R., Chen X. A new scheme for source term in LBGK model for convection-diffusion equation. Computers & Mathematics with Applications. **55** (7), 1568–1575 (2008).

[17] Chai Z., Zhao T. S. Lattice Boltzmann model for the convection-diffusion equation. Physical Review E. **87** (6), 063309 (2013).

[18] Chaabane R., Askri F., Nasrallah S. B. Analysis of two-dimensional transient conduction?radiation problems in an anisotropically scattering participating enclosure using the lattice Boltzmann method and the control volume finite element method. Computer Physics Communications. **182** (7), 1402–1413 (2011).

[19] Jawerth B., Lin P., Sinzinger E. Lattice Boltzmann Models for Anisotropic Diffusion of Images. Journal of Mathematical Imaging and Vision. **11**, 231–237 (1999).

[20] Sun X., Wang Z., Chen G. Parallel active contour with Lattice Boltzmann scheme on modern GPU. 2021 19th IEEE International Conference on Image Processing. 1709–1712 (2012).

[21] Balla-Arabé S., Gao X. Image multi-thresholding by combining the lattice Boltzmann model and a localized level set algorithm. Neurocomputing. **93**, 106–114 (2012).

[22] Chang Q., Yang T. A Lattice Boltzmann Method for Image Denoising. IEEE Transactions on Image Processing. **18** (12), 2797–2802 (2009).

[23] Chen J., Chai Z., Shi B., Zhang W. Lattice Boltzmann method for filtering and contour detection of the natural images. Computers & Mathematics with Applications. **68** (3), 257–268 (2014).

[24] Ambrosio L., Tortorelli V. M. Approximation of functional depending on jumps by elliptic functional via t-convergence. Communications on Pure and Applied Mathematics. **43** (8), 999–1036 (1990).

[25] Nomura A., Ichikawa M., Sianipar R. H., Miike H. Edge detection with reaction-diffusion equations having a local average threshold. Pattern Recognition and Image Analysis. **18** (2), 289–299 (2008).

[26] Witkin A., Kass M. Reaction-diffusion textures. ACM SIGGRAPH Computer Graphics. **25** (4), 299–308 (1991).

[27] Sanderson A. R., Johnson C. R., Kirby R. M., Yang L. Advanced reaction-diffusion models for texture synthesis. Journal of Graphics Tools. **11** (3), 47–71 (2006).

[28] Black M. J., Sapiro G., Marimont D. H., Heeger D. Robust anisotropic diffusion. IEEE Transactions on Image Processing. **7** (3), 421–432 (1998).

Новий метод граткових рівнянь Больцмана для базової моделі Грея–Скотта, застосований для відновлення зображень та покращення їхнього контрасту

Ала Х.[1], Ала Н. Е.[1], Акель Ф.[2], Лефрайх Х.[3]

[1]*Лабораторія LAMAI, факультет науки і технологій Університету Каді Айяда, 40000 Марракеш, Марокко*

[2]*Лабораторія комп'ютерів, мереж, мобільності та моделювання (IR2M), факультет наук і техніки Першого університету Хасана в Settаті, B.P. 577, Settат 26000, Марокко*

[3]*Лабораторія MISI, факультет наук і техніки, Перший університет Хасана в Settаті, B.P. 577, Settат 26000, Марокко*

Мета цієї роботи — запропонувати новий чисельний підхід до відновлення зображення та покращення його контрасту на основі реакційно-дифузійної моделі (модель Грея–Скотта). Для видалення шумів використовується методика граткових рівнянь Больцмана. Зазвичай вона використовується в експериментах з гідродинаміки. Оскільки рух пікселів можна порівняти з рухом рідини, представлена методика демонструє хорошу продуктивність при обробці зашумлених зображень. Ефективність та продуктивність запропонованого алгоритму перевірено на кількох чисельних експериментах.

Ключові слова: *відновлення зображення, метод граткових рівнянь Больцмана, модель Грея—Скотта, реакція–дифузія, покращення контрасту, схема $D2Q9$, схема $D2Q5$.*